Damping control for improvement of acoustic black hole effect

Morvan Ouisse, David Renault, Pauline Butaud, Emeline Sadoulet

Damping control for improvement of acoustic black hole effect

Morvan Ouisse, David Renault, Pauline Butaud, Emeline Sadoulet-Reboul[1]

Univ. Bourgogne Franche Comté, FEMTO-ST Institute, CNRS/UFC/ENSMM/UTBM, Department of Applied Mechanics, 24 rue de l'épitaphe, 25000 Besançon, France

Abstract

Acoustic Black Holes are innovative solutions to damp vibrations through the use of power-law profiles in flexural beams and plates. However practical implementations of the concept are limited due to the finiteness of the thickness at the end of the beam. In this paper, it is proposed to add a viscoelastic layer on the ABH and control its mechanical properties by varying the temperature of the material in order to obtain an ABH with tunable properties. A design methodology of the damping layer is proposed, based on the computation of the reflection coefficient of the ABH termination, hence independent from the excitation and the boundary conditions of the host structure. This optimization is performed at a temperature close to the glass transition of the viscoelastic material in order to find the configuration providing the highest dissipation. Then, by controlling the temperature of the patch it is easy to tune the behavior of the ABH according to the practical application which is considered.

Keywords: Acoustic black hole, Vibration black hole, Damping control, Thermal control

1. Introduction

Damping flexural vibration of thin structures can be obtained through various means, including the use of the so-called Acoustic Black Hole (ABH) effect

[1]Corresponding author: Morvan Ouisse (morvan.ouisse@femto-st.fr)

[1, 2, 3], which is obtained by tailoring the structure boundaries using power-law profiles. A perfect thickness profile would decrease the wave velocity asymptotically to zero, meaning that the edge is never reached hence the wave is not reflected. This theoretical behaviour is however difficult to obtain because of manufacturing constraints which impose a non-zero thickness at the border, inducing some reflections of flexural waves. Using a damping layer [4] may be a solution to damp the waves in the black hole, even if this is not mandatory since local imperfections at the edge may induce dissipation through nonlinear effects [5].

The applicability of the concept has been demonstrated by several authors [6, 7, 8], mostly for metallic structures, but also for glass fibre composite plates [9]. New designs have been proposed recently, like spiral arrangements of the ABH to minimize the size of the device [10], or novel dampers tailored with ABH features [11]. The emergence of these upgraded ABH-based devices probably motivated some groups to imagine other applications than structural damping. Hence, new applications of the ABH concept have emerged: among others, energy harvesting [12] and wave energy focalization [13] are good examples of concepts that can take advantage of the unusual mechanical properties of ABH.

Up to now, to the author's knowledge, real-time tunables ABH have not been proposed in open literature. The work presented here is devoted to the analysis of beams embedding an ABH whose damping properties can be tuned in real time. The concept is based on temperature control of the viscoelastic properties of a damping layer [14]. This adaptive concept is different from active devices [15, 16] in the sense that the time scale required in the temperature regulation is much smaller than the one of the phenomena to be controlled. It may however be qualified as semi-active [17, 18] since some energy is required to heat the damping layer according to the objectives. The aim of the heat control is to tune the mechanical properties of the viscoelastic material: it is well known for years that their stiffness and damping properties are strongly dependent on frequency and temperature [19, 20, 21]. Many works hence focused on the effect of the temperature on the structural damping performances [22, 23, 24] or on the

optimization of the viscoelastic properties for a given ambient temperature [25]. Here, the concept of temperature control is considered. It has been introduced recently [14] and will be applied here to tune the mechanical properties of the embeded viscoelastic layer in the ABH-based structure. This concept has been recently successfully applied to metamaterials [26] for tuning the stiffness of a periodic structure, here the objective is rather focused on the tuning of the damping properties that directly impact the performances of the ABH.

The paper is organized as follows. Section 2 introduces the structure of interest, namely a beam embedding an ABH combined with a damping layer. Section 3 presents the concept of temperature control of the mechanical properties of the viscoelastic material and its application to the structure. Section 4 presents the optimization strategy which has been developed in order to define the optimal configuration for given performances. Section 5 finally illustrates the applicability of the concept through experimental validations, and conclusions are drawn.

2. ABH combined with damping layer

The Acoustic Black Hole which is considered in this paper is located at the end of a host beam. The host beam is made of aluminum (Young's modulus $E = 70000$ MPa, density $\rho = 2700$ kg/m^3, loss factor $\eta = 0.002$), its thickness is $h_0 = 5$ mm and its width is 2 cm. The damping effect is increased by a viscoelastic layer which is glued on the ABH. Figure 1 illustrates the beam and its termination. The numerical values of the host beam parameters are provided in Table 1. The properties of the viscoelastic layer (including h_v and L_v) will be discussed all along this paper.

As stated in [4], the effect of the damping layer located at the end of the ABH helps to reduce the reflections due to the finite thickness of the termination. This is numerically illustrated in the Fig. 3. Like all numerical results presented in this paper, the computations have been performed on a 2D finite element model in the $(\vec{x}, \vec{y})$ plane of Fig. 3, using 694 quadratic plane strain elements. Fig. 2

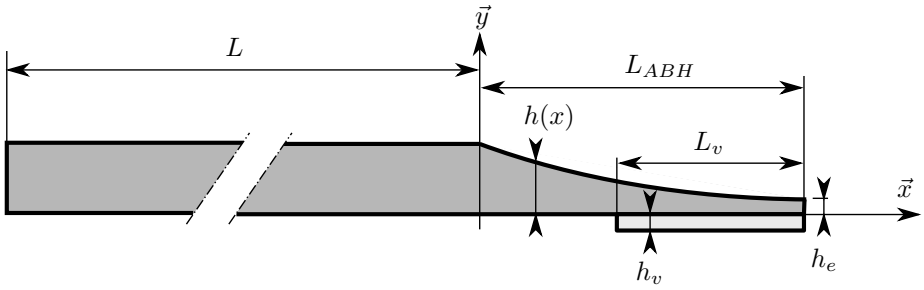

Figure 1: ABH with damping layer

L	54 cm
L_{ABH}	15 cm
h_e	89 μm
$h(x)$	$h_0 \left(\frac{L_{ABH} - x}{L_{ABH}} \right)^2$

Table 1: Numerical values of the parameters of the host beam

shows two views of the ABH with damping layer finite element mesh.

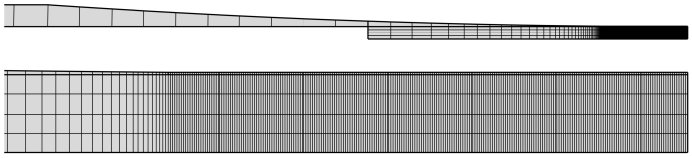

Figure 2: Two views of the finite element mesh (ABH and its end)

According to the experimental configuration that will be discussed later, the beam is considered as free-free, a harmonic force F is applied along $\vec{y}$ direction at a point located at 1 cm from the non-ABH termination of the beam (*ie* $x = -L + 1$cm in figure 3). The transverse velocity v is computed at the input force location. The amplitude of the mobility v/F is shown in figure 3.

In this first analysis and for illustration purpose, the damping layer is constituted by a virtual material ($h_v = 1$ mm and $L_v = 15$ cm, Young's modulus $E_v = 3$ MPa, density $\rho_v = 900$ kg/m^3, loss factor $\eta_v = 0.8$, considered constant in frequency).

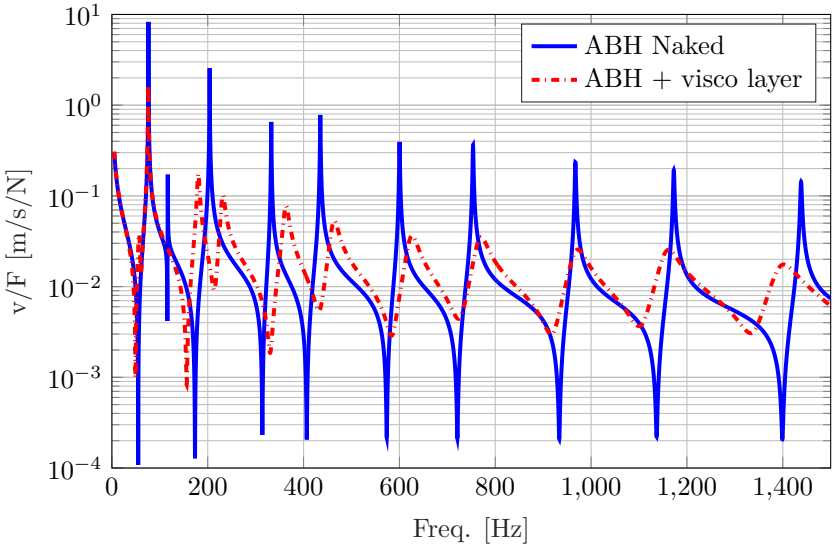

Figure 3: Simulation results - Mobility comparison between ABH with/without viscoelastic layer (constant damping properties in frequency)

As expected, the damping layer plays a major role in the efficiency of the ABH since it helps to dissipate the energy which is reflected on the non-zero thickness termination. The mobility curve is quite illustrative but dependent on the host beam and input force location. A more general property is the reflection coefficient, which is independent of the length and boundary conditions used on the host beam. Based on the generic analytical expression of the transverse displacement of an Euler-Bernoulli beam

$$w(x) = Ae^{-jkx} + Be^{jkx} + Ce^{-kx} + De^{kx} \tag{1}$$

where k is the flexural wave number and A, B, C, D are constants that depend on the boundary conditions, the reflection coefficient is expressed as

$$R = \frac{B}{A} \tag{2}$$

since the ABH starts at $x = 0$. It represents the amplitude of the propagative waves that are reflected on the ABH, which can be interpreted as a complex, frequency-dependent boundary condition for the host beam. It only depends

on the ABH characteristics. In this paper, it is computed from the technique proposed in [27], consisting in measuring the transverse displacement $w(x_i)$ at n locations x_i along the beam ($i = 1, ..., n \geq 2$), computing the wave number from the analytical formula and using pseudo-inverse to estimate A and B coefficients from the matrix system

$$\begin{bmatrix} e^{-jkx_1} & e^{jkx_1} \\ ... & ... \\ e^{-jkx_n} & e^{jkx_n} \end{bmatrix} \begin{Bmatrix} A \\ B \end{Bmatrix} = \begin{Bmatrix} w(x_1) \\ ... \\ w(x_n) \end{Bmatrix}. \tag{3}$$

This approach is valid if the flexural movement of interest is the only one contributing to the measured values $w(x_i)$ (in particular, the torsion movement should not appear in the measurement, meaning that sensors should be located in the middle of the width of the beam), but also if the evanescent waves (described by C and D) are negligible at the measurement points, meaning that they should be located far from the force location or any discontinuity in the host beam. A practical rule consists in avoiding measurement at a distance lower than the quarter of the wavelength. In the whole paper, this technique has been used with 3 measurement points located at $x_1 = -17.5$ cm, $x_2 = -20$ cm and $x_3 = -25$ cm. Numerical simulations considering both propagative and evanescent waves in the estimation of A and B have been performed to check the validity of the hypothesis.

The modulus of the reflection coefficient computed with this technique is shown in figure 4 where it can clearly be observed that the viscoelastic layer has a very important effect on the reflection coefficient and dissipates the energy, while the non-zero termination of the ABH without damping layer reflects almost all the energy, the dissipation occurring only through the loss factor of the host material.

Finally, it may be stated that a part of the flexural energy could be converted in longitudinal vibrations since the structure is not symmetric. This conversion is described in the finite element model and only small amplitude in the longitudinal displacements have been observed, due to the fact that the damping

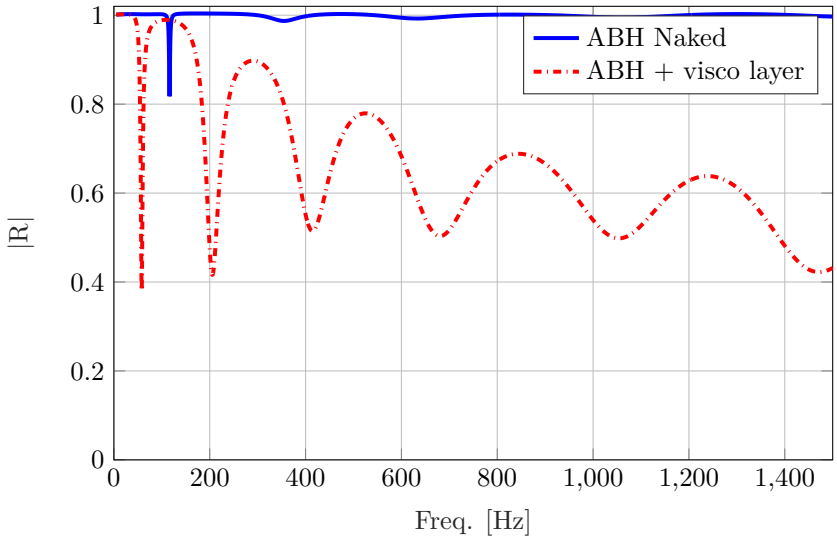

Figure 4: Simulation results - reflection coefficient comparison between ABH with/without viscoelastic layer (constant damping properties in frequency)

layer dissipates the associated energy.

3. Temperature control of damping in viscoelastic layer

The objective of this section is to show that the ABH effect can be tuned with a temperature control of a viscoelastic layer. The material is a tBA/PEGDMA polymer (named SMP in the following since it is a Shape Memory Polymer) whose behavior can be efficiently described by the model provided in [14]. The model is representative of the set of experiments presented in [28]. This viscoelastic material has strongly dependent mechanical properties, in particular the loss factor can be as high as 2.4 at the glass transition, occurring around 70°C. Using arbitrary length and thickness, the effect of the temperature control on the reflection coefficient of the ABH equipped with the SMP is illustrated in figure 5.

At ambiant temperature, the loss factor of the material is very low and the SMP dissipates only a few energy. When the temperature of the material is increased, the effect on the reflection coefficient is becoming more important: the

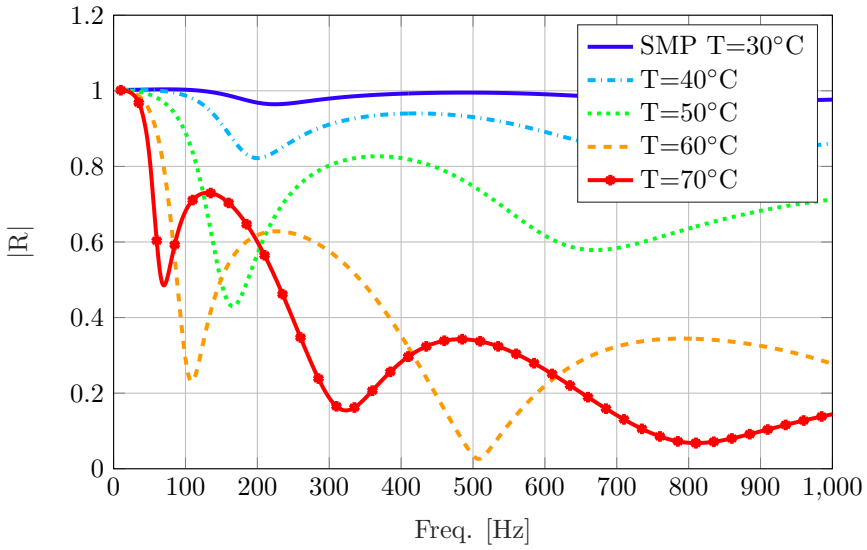

Figure 5: Simulation results - reflection coefficient of the ABH equipped with the SMP layer, for various temperatures

first minimum of the reflection coefficient occurs at a lower frequency, and its mean value is also decreasing, at least up to 60°C. Depending on the frequency range on which the mean is computed, the most dissipative configuration among the simulated cases corresponds either to 60°C or 70°C. The figure clearly illustrates the fact that the mechanical properties of the ABH can be tuned by temperature control.

The next section presents the optimization procedure which has been used to choose the length and thickness of the damping layer.

4. Optimal design of the damping layer

Designing a damping layer always consists in finding a compromise between damping and stiffness, this is particularly true for the considered case since the added layer will increase the stiffness of the ABH section and hence it is expected that it will affect its performances. The added value provided by the dissipation should bring more benefits than the decrease of performance due to

the added stiffness.

In order to find the optimal design for the damping layer, a parametric model-based study has been performed. As illustrated above, the damping capability of the SMP is the most efficient for a temperature close to the glass transition which occurs between 60° and 70°C.

During this optimization procedure, the temperature was fixed to 70°C and two geometrical parameters were considered, namely thickness (h_v) and width of the SMP layer (L_v). Thickness is considered in the range 0.3 mm to 3 mm. The width is considered relatively to the ABH length and varies from 0.25 to $1.5 : 1$ consist in a exact covering of the termination while 0.25 consist of 25 percent covering from the free end of the ABH.

Several numerical indicators can be considered to quantify the performances of the designs. A first approach based on the study of the admittance curves (figure 3) can be suggested: the peaks of the mobility curve can be detected, the amplitude and damping (evaluated using a bandwidth approach) may be identified and used as features that characterize the damping. This approach provides good indications of the evolution of the damping but is not easy to implement for a full automation: the number of peaks in the frequency range may vary and the value of the modal damping factor calculated with bandwidth approach is sometimes uncertain when the curves are very smooth (see for example the red curve in figure 3 or more clearly later in figure 8), corresponding to highly damped configurations.

To improve this, a global approach considering the mean value of the amplitude of the reflection coefficient over the frequency range of interest was used. Using this feature a non-damped system gives a feature value near 1 and the objective of the optimization procedure consists in minimizing this feature. Results are consistent between the two approaches but the second one is easier to deal with since first, the post-processing of the mobility curve is not required, and second, a single numerical feature is required while the first approach requires to combine all modal information in the frequency range. Moreover, the optimization becomes independent from the location of the excitation force and

from the boundary conditions. Alternative objective functions may have been used to characterize the performances of the device, like indicators associated to the dissipated energy in the damping layer, that would probably provide similar trends.

For the considered ABH application, the indicator was evaluated on two frequencies ranges (0-200 Hz and 0-1000 Hz) in order to find the best design for the full range and check the consistency with results computed only for the lower frequencies. As only two geometrical parameters are studied, it is possible to perform a full factorial design of experiment with large number of levels and plot the corresponding indicator as a response surface. Figure 6 shows the two response surfaces corresponding to the two frequency ranges.

As seen in the figures, the optimal configuration is not exactly the same for the two frequency ranges: the thickness is 3 mm for both cases, while the relative width is close to 0.4 for the wide frequency range and close to 0.6 for the 0-200 Hz analysis. In the following, the compromise corresponding to 50 percent covering of the ABH ending has been used.

Using this optimal geometrical design, some simulations were performed in order to show the ability of the SMP to control damping behavior using temperature. The mean value of the reflection coefficient was computed for the two frequency ranges (0-1000 Hz and 0-200 Hz) for various temperatures. The evolution plots, shown in figure 7), show that for the largest frequency range a steady state is reached for temperatures above 70°C. For the lower frequency range, a minimum is found near 70°C. These curves illustrate that the damping effect of the SMP becomes very important when the temperature increases over 50°C and becomes optimal near 70°C.

In order to illustrate these results, mobilities and reflection coefficient curves are plotted for the optimal geometrical parameters, for temperatures from 30°C to 90°C with a 10°C step in figure 8 and 9.

As expected, both the mobility and reflection coefficient show the efficiency of the temperature control for tuning the damping in the ABH: by changing the temperature of the SMP, we can pass from a quasi purely reflective configuration

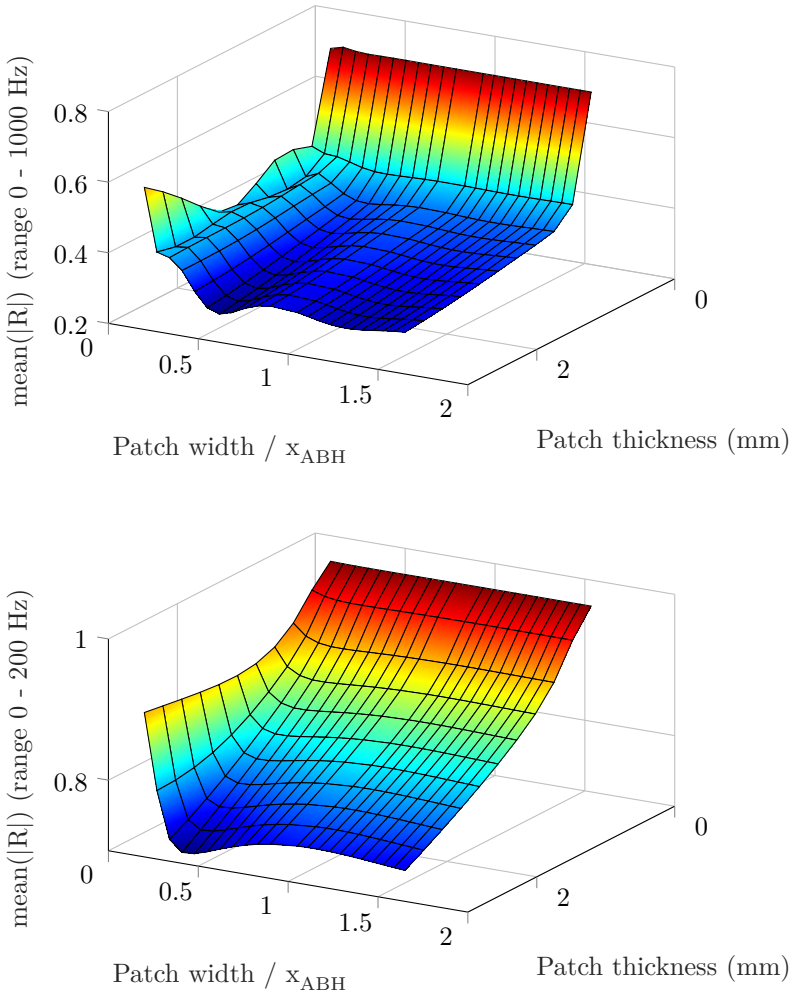

Figure 6: Response surfaces plotted using the full factorial design of experiments results: mean value of reflection coefficient amplitude vs. relative patch width and patch thickness. Upper figure: computation on 0-1000 Hz; lower figure: computation on 0-200 Hz.

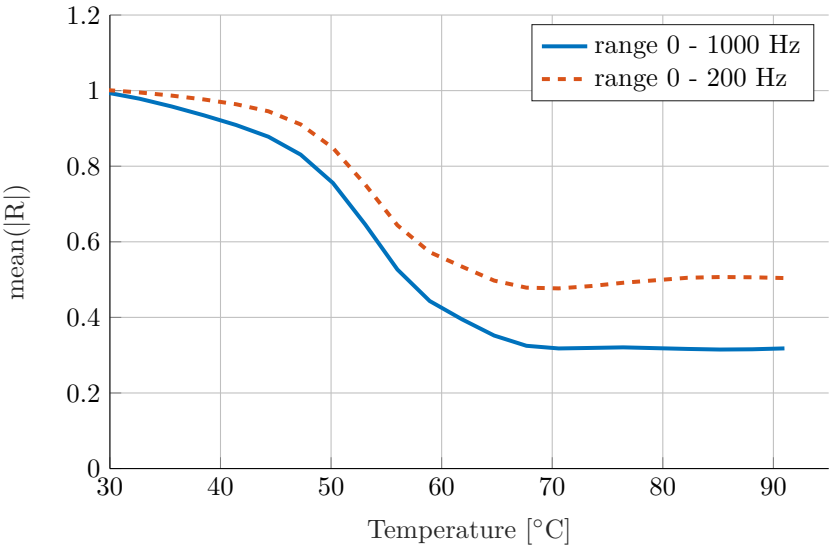

Figure 7: Evolution of mean integral value of the reflection coefficient with temperature

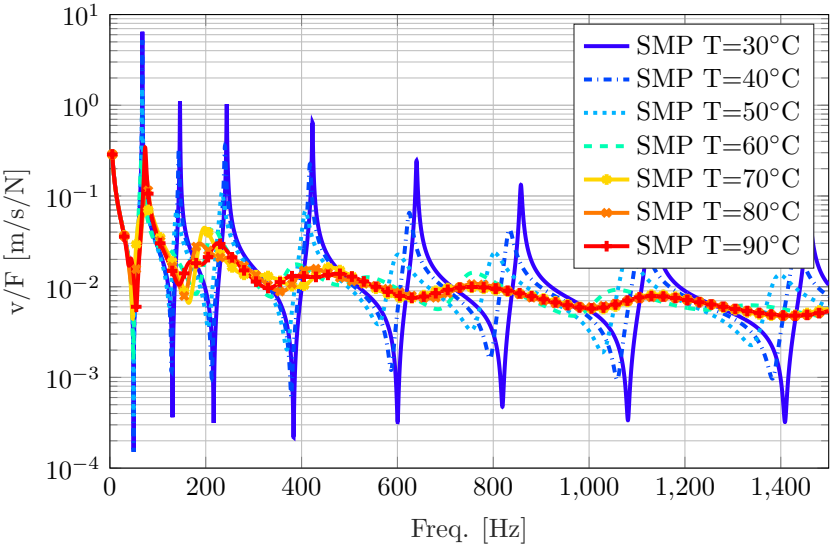

Figure 8: Simulation results - amplitude of the mobility for the optimal configuration at various temperatures

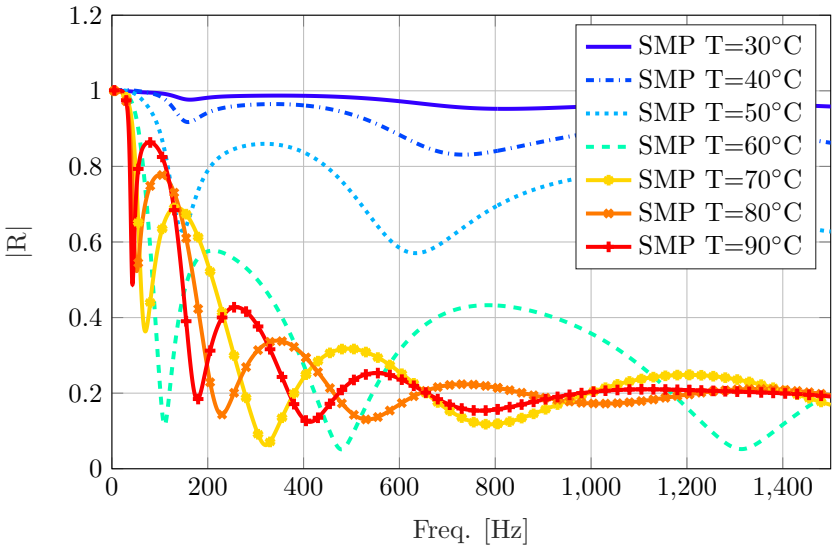

Figure 9: Simulation results - amplitude of reflection coefficient for the optimal configuration at various temperatures

(at ambiant temperature) to a highly absorptive configuration. High dissipation levels are obtained above 50°C and up to 90°C, corresponding to various wide band effects that can be chosen according to the application of interest.

5. Experimental validation

This section is dedicated to the experimental validation of the concepts presented above. The ABH beam has been provided by LAUM-Le Mans University, while the damping layer has been elaborated in FEMTO-ST-University Bourgogne Franche-Comté, according to the optimal configuration . A picture of the termination is shown in figure 10.

The experimental setup is shown in figure 11. The beam is suspended with thin wires inside a thermal chamber to approximate free-free boundary conditions. The excitation force is generated by a contactless actuator, consisting in a fixed coil accompanied with a magnet glued on the beam. An impedance head is used to measure the mobility and to check the coherence with the accelerom-

Figure 10: View of the ABH termination with SMP layer

eters which have been used to estimate the reflection coefficient. White noise is used to excite the beam. For each tested temperature, the measurements are performed after 10 minutes in order to be sure that the SMP is uniformly heated. For practical applications of the concept, heating layers can easily be implemented inside the viscoelastic layer or at its surface.

The figure 12 shows the reflection coefficients identified from the measurements for the same set of temperatures as the one used for the simulations. The experimental data are a little bit noisy, this is mostly due to non-perfect alignment of point force and accelerometers on the median line of the beam, hence parasitic movements like torsion or in-plane bending may occur. Also, the accelerometers (B&K miniature accelerometers were used) may generate evanescent components in the displacement field which are not considered in the evaluation of the reflection coefficient. The noise could probably be reduced by using a scanning laser vibrometer to be able to measure a large set of points without perturbation on the beam. Nevertheless, the trends observed in figure 9 are perfectly reproduced in the experiment.

A direct comparison between numerical and experimental results is shown

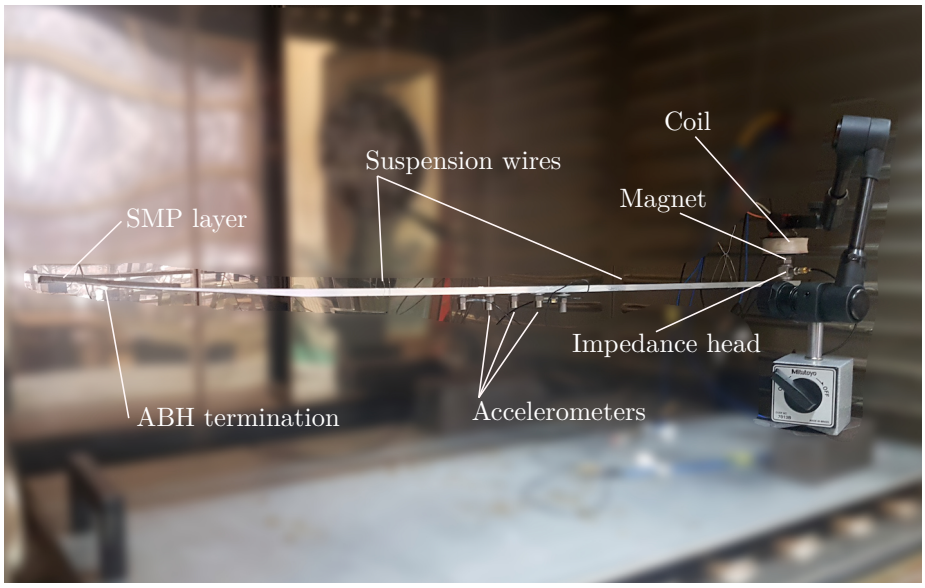

Figure 11: Experimental setup - host beam with ABH and damping layer suspended in the thermal chamber

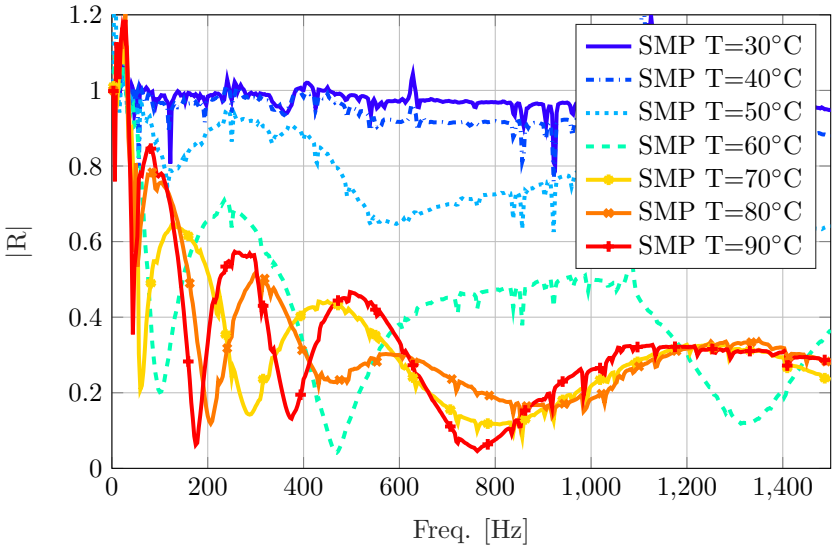

Figure 12: Experimental results - amplitude of reflection coefficient for optimal configuration at various temperatures

in figures 13 and 14. The temperatures set is split in two parts to enhance the readability of the figures.

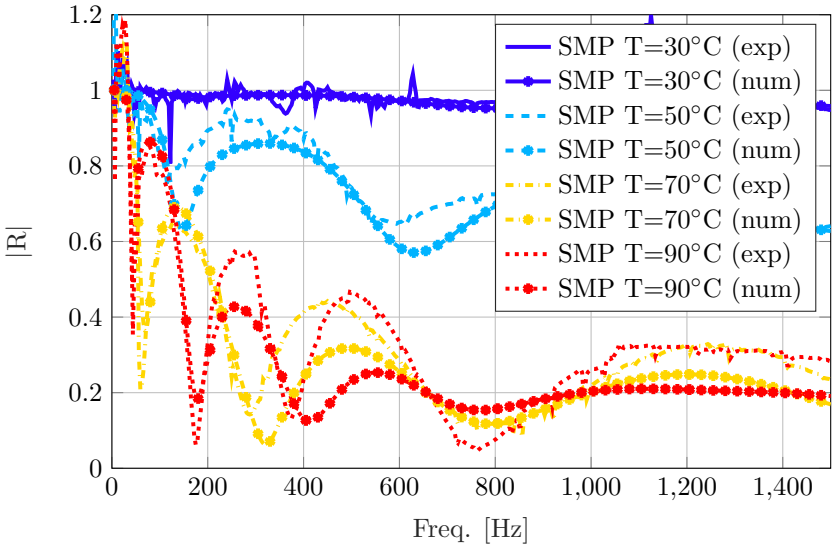

Figure 13: Comparison of amplitude of reflection coefficients for optimal configuration at various temperatures

As seen in the figures, the correlation between the model and the experimental results is very good on the whole set of temperatures. The discrepancies are becoming larger when the temperature is close to the glass transition because in this range the elastic modulus and the loss factor of the SMP are very sensitive to the temperature. The uncertainty associated to the temperature probe is 2°, corresponding to a factor up to 2 on the loss factor and over 3 on the elastic modulus at the glass transition. Also, it may be mentioned that the geometry of the manufactured ABH is not perfect, for example the thickness of the termination has been measured at 0.17mm instead of 0.089 as expected. This obviously may impact the precision of the model. However the overall correlation is very good and the model can be confidently used to design practical applications taking advantage of the temperature tuning of the damping level in ABHs.

The mean values of these experimental reflection coefficients can be computed and compared to the numerical ones. This is done in figure 15. Again,

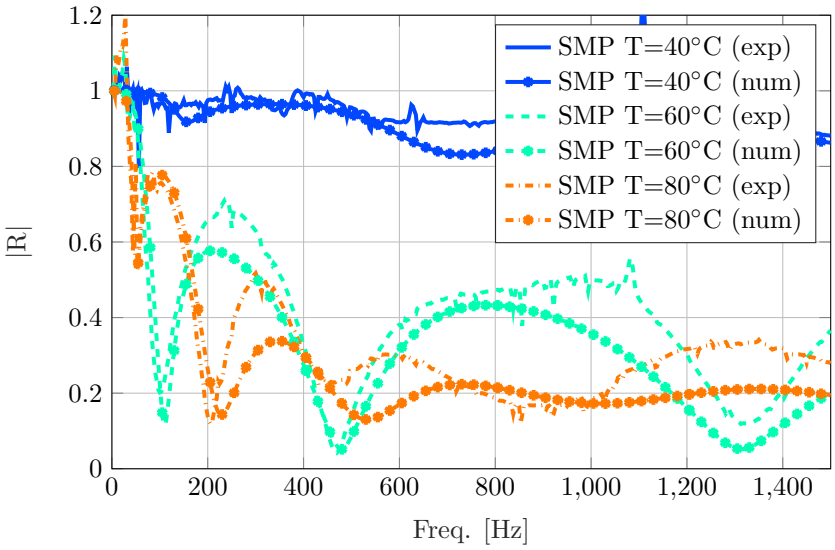

Figure 14: Comparison of amplitude of reflection coefficients for optimal configuration at various temperatures

the correlation is excellent. Only the experimental values above 60° overestimate the mean value of the reflection coefficient computed on the 0-200 Hz range. This may be explained by the non-physical values of R at very low frequency: below 25 Hz, its amplitude exceeds unity probably because of the suspension wires which are not perfectly soft.

Finally, figure 16 illustrates the efficiency of the damping tuning on the mobility function. The trends are perfectly in accordance with the numerical model, confirming the applicability of the concept. The amplitudes of the resonances are not as high as those predicted by the model. This is due to the excitation procedure, which uses a magnet-coil, hence the movement of the beam induces a Laplace force in the magnetic field, which is proportional and in opposition to the velocity, hence acting like a local viscous damper. This explains the higher damping level observed for the low temperatures, when the SMP dissipation capabilities are not activated yet. The resonance frequencies are also a little bit shifted compared to the numerical model. This is due to the added masses (accelerometers and magnets) and to the boundary conditions which are not

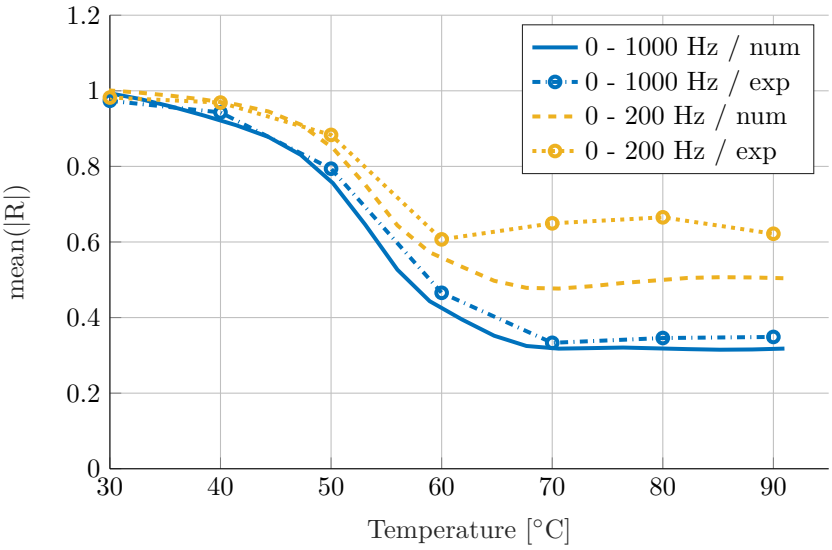

Figure 15: Evolution of mean integral value of the reflection coefficient with temperature, comparison between experiments and simulations

strictly free. However, it is interesting to note that the proposed methodology being based on the reflection coefficient of the ABH, it is independent from the excitation and the boundary conditions: the reflection coefficient is only affected by the ABH zone (*ie* $x > 0$). The same ABH with damping layer applied on another beam would have the same reflection coefficient but different mobility.

6. Conclusion

In this paper, it has been shown that it was possible to control the damping in order to improve the acoustic black hole effect. This is achieved through the use of a viscoelastic layer whose properties are tuned by temperature control. The ABH is equipped with a patch of polymer, whose dimensions can be optimized to maximize the damping effect at a temperature close to the glass transition, on the basis of the mean value of the amplitude of the reflection coefficient, computed on the frequency range of interest. This renders the methodology independent from the excitation and the boundary conditions of

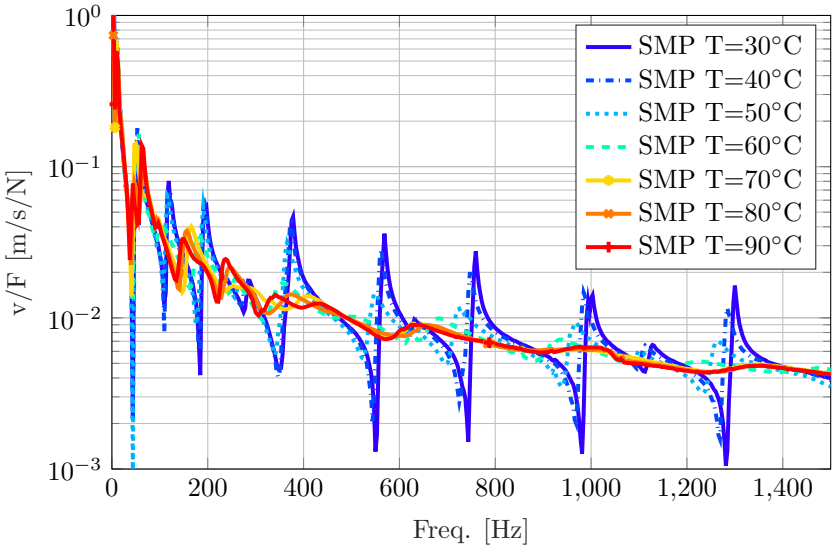

Figure 16: Experimental results - amplitude of mobility on the host beam with ABH for the optimal configuration at various temperatures

the host structure. Then, by controlling the temperature of the patch it is easy to tune the behavior of the ABH according to the practical application which is considered. In this work, the tBA/PEGDMA -a Shape Memory Polymer- has been used, however the methodology may be applied with any viscoelastic material exhibiting a strong depedency on temperature. In order to illustrate this, figure 17 shows the experimental measurements performed with another material, which is available off-the-shelf (3M VHB). This material is more efficient than the SMP at ambiant temperature for the damping, and a little less efficient at high temperature. Hence it could constitute an interesting alternative for applications where either the damping does not have to be tuned (in particular if the temperature is around 20-30°). On the other hand, for a tunable system that can be changed in real time from reflective to dissipative, the proposed SMP will constitute a good candidate.

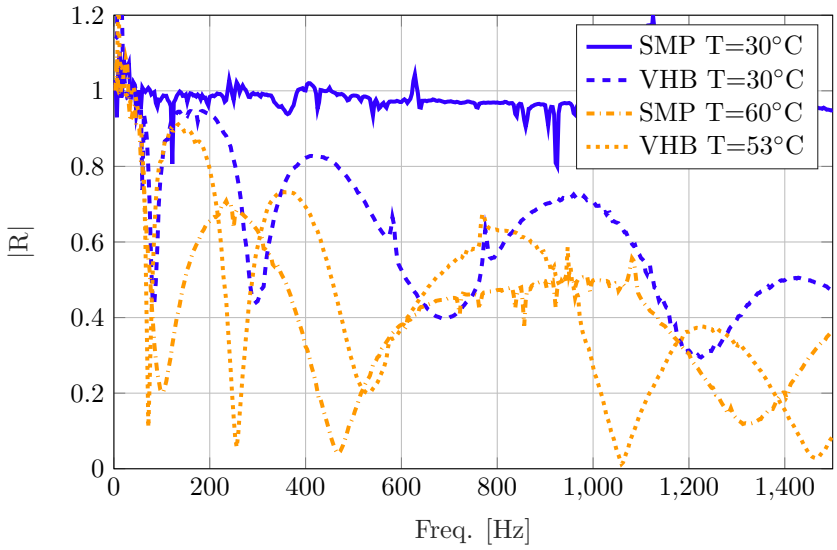

Figure 17: Experimental results - amplitude of reflection coefficient, comparison SMP / VHB

Acknowledgements

The authors would like to thank François Gautier and Adrien Pelat (Le Mans University, France) for the fruitful discussions and for providing the host beam with the ABH. This work has been funded by ANR (contract ANR-17-CE08-0035 ETNAA), in collaboration with EIPHI Graduate School (ANR-17-EURE-0002).

References

[1] M. Mironov, Propagation of a flexural wave in a plate whose thickness decreases smoothly to zero in a finite interval, Soviet Physics Acoustics-USSR 34 (3) (1988) 318–319.

[2] V. Krylov, F. Tilman, Acoustic 'black holes' for flexural waves as effective vibration dampers, Journal of Sound and Vibration 274 (3-5) (2004) 605–619.

[3] V. Georgiev, J. Cuenca, F. Gautier, L. Simon, V. Krylov, Damping of structural vibrations in beams and elliptical plates using the acoustic black hole effect, Journal of sound and vibration 330 (11) (2011) 2497–2508.

[4] J. Cuenca, A. Pelat, F. Gautier, N. Ferguson, Improving the acoustic black hole effect for vibration damping in one-dimensional structures, in: Acoustics 2012, Nantes (France), 2012.

[5] V. Denis, A. Pelat, F. Gautier, Scattering effects induced by imperfections on an acoustic black hole placed at a structural waveguide termination, Journal of Sound and Vibration 362 (2016) 56–71.

[6] E. Bowyer, V. V. Krylov, Damping of flexural vibrations in turbofan blades using the acoustic black hole effect, Applied Acoustics 76 (2014) 359–365.

[7] S. C. Conlon, J. B. Fahnline, F. Semperlotti, Numerical analysis of the vibroacoustic properties of plates with embedded grids of acoustic black holes, The Journal of the Acoustical Society of America 137 (1) (2015) 447–457.

[8] L. Tang, L. Cheng, Enhanced acoustic black hole effect in beams with a modified thickness profile and extended platform, Journal of Sound and Vibration 391 (2017) 116–126.

[9] E. Bowyer, V. V. Krylov, Experimental investigation of damping flexural vibrations in glass fibre composite plates containing one-and two-dimensional acoustic black holes, Composite Structures 107 (2014) 406–415.

[10] J. Y. Lee, W. Jeon, Vibration damping using a spiral acoustic black hole, The Journal of the Acoustical Society of America 141 (3) (2017) 1437–1445.

[11] T. Zhou, L. Cheng, A resonant beam damper tailored with acoustic black hole features for broadband vibration reduction, Journal of Sound and Vibration 430 (2018) 174–184.

[12] L. Zhao, S. C. Conlon, F. Semperlotti, Broadband energy harvesting using acoustic black hole structural tailoring, Smart materials and structures 23 (6) (2014) 065021.

[13] W. Huang, H. Ji, J. Qiu, L. Cheng, Wave energy focalization in a plate with imperfect two-dimensional acoustic black hole indentation, Journal of Vibration and Acoustics 138 (6) (2016) 061004.

[14] P. Butaud, E. Foltête, M. Ouisse, Sandwich structures with tunable damping properties: on the use of shape memory polymer as viscoelastic core, Composite Structures 153 (2016) 401–408. doi:10.1016/j.compstruct.2016.06.040.

[15] C. C. Fuller, S. Elliott, P. A. Nelson, Active control of vibration, Academic Press, 1996.

[16] D. J. Inman, Vibration with control, John Wiley & Sons, 2017.

[17] M. Collet, M. Ouisse, F. Tateo, Adaptive metacomposites for vibroacoustic control applications, IEEE Sensors Journal 14 (6). doi:10.1109/JSEN.2014.2300052.

[18] M. Ouisse, M. Collet, F. Scarpa, A piezo-shunted kirigami auxetic lattice for adaptive elastic wave filtering, Smart Materials and Structures 25 (2016) 115016. doi:10.1088/0964-1726/25/11/115016.

[19] M. Caputo, F. Mainardi, Linear models of dissipation in anelastic solids, La Rivista del Nuovo Cimento (1971-1977) 1 (2) (1971) 161–198.

[20] J. D. Ferry, J. D. Ferry, Viscoelastic properties of polymers, John Wiley & Sons, 1980.

[21] R. S. Lakes, Viscoelastic solids, Vol. 9, CRC press, 1998.

[22] K.-C. Chang, T. Soong, S.-T. Oh, M. Lai, Effect of ambient temperature on viscoelastically damped structure, Journal of Structural Engineering 118 (7) (1992) 1955–1973.

[23] Y. Sefrani, J.-M. Berthelot, Temperature effect on the damping properties of unidirectional glass fibre composites, Composites Part B: Engineering 37 (4-5) (2006) 346–355.

[24] G. A. Lesieutre, K. Govindswamy, Finite element modeling of frequency dependent and temperature-dependent dynamic behavior of viscoelastic materials in simple shear, International Journal of Solids and Structures 33 (3) (1996) 419–432.

[25] P. Millithaler, J.-B. Dupont, M. Ouisse, E. Sadoulet-Reboul, N. Bouhaddi, Viscoelastic property tuning for reducing noise radiated by switched-reluctance machines, Journal of Sound and Vibration 407 (2017) 191–208. doi:10.1016/j.jsv.2017.07.008.

[26] K. Billon, M. Ouisse, E. Sadoulet-Reboul, M. Collet, P. Butaud, G. Chevallier, A. Khelif, Design and experimental validation of a temperature-driven adaptive phononic crystal slab, Smart Materials and Structuresdoi:10.1088/1361-665X/aaf670.

[27] V. Denis, F. Gautier, A. Pelat, J. Poittevin, Measurement and modelling of the reflection coefficient of an acoustic black hole termination, Journal of Sound and Vibration 349 (2015) 67–79.

[28] P. Butaud, M. Ouisse, V. Placet, F. Renaud, T. Travaillot, A. Maynadier, G. Chevallier, F. Amiot, P. Delobelle, E. Foltête, C. Rogueda-Berriet, Identification of the viscoelastic properties of the tBA/PEGDMA polymer from multi-loading modes conducted over a wide frequency–temperature scale range, Polymer Testingdoi:10.1016/j.polymertesting.2018.05.030.